CHALMERS
UNIVERSITY OF TECHNOLOGY

Design of Contactless D-Band MMIC-to-Waveguide Transition Based on Multilayer Waveguide and SiGe Technology

Downloaded from: https://research.chalmers.se, 2026-06-18 10:35 UTC

Citation for the original published paper (version of record):
Chang, H., He, Z., Vassilev, V. et al (2026). Design of Contactless D-Band MMIC-to-Waveguide Transition Based on Multilayer Waveguide and
SiGe Technology. IEEE Microwave and Wireless Technology Letters, In Press.
http://dx.doi.org/10.1109/LMWT.2026.3696765

N.B. When citing this work, cite the original published paper.

© 2026 IEEE. Personal use of this material is permitted. Permission from IEEE must be obtained for all other uses, in any current or future media, including reprinting/republishing this material for advertising or promotional purposes, or reuse of any copyrighted component of this work in other works.

(article starts on next page)

This article has been accepted for inclusion in a future issue of this journal. Content is final as presented, with the exception of pagination.

Design of Contactless D-Band MMIC-to-Waveguide Transition Based on Multilayer Waveguide and SiGe Technology

Haojie Chang, *Member, IEEE*, Zhongxia Simon He, *Senior Member, IEEE*, Vessen Vassilev, Frida Strömbeck, *Member, IEEE*, Yu Yan, *Member, IEEE*, and Herbert Zirath, *Life Fellow, IEEE*

***Abstract*—A D-band transition from silicon–germanium (SiGe) monolithic microwave integrated circuit to waveguide (MMIC-WG) is proposed in this letter. The transition includes a slot etched in the chip's ground plane and a two-stage step in a metal waveguide. The slot works as a launcher for contactless electromagnetic field coupling, fed by a shorted microstrip line, while the step is an impedance transformer. As the assembly requires splitting the waveguide along the H-plane, glide-symmetric holes in a multilayer waveguide (MLW) are introduced as an electromagnetic bandgap (EBG) structure to suppress leakage, different from metal pins used in an H-split rectangular waveguide (RWG). As a proof of concept, a back-to-back (B2B) transition is fabricated based on MLW technology with an additional H-split RWG design as a reference. Measurement results show the proposed transitions have 2-dB insertion loss, in good agreement with the simulation. In addition, packaged receivers are also presented to validate the feasibility of the proposed transitions for sub-THz system integration.**

***Index Terms*—Back-to-back (B2B), D-band monolithic microwave integrated circuit to waveguide (MMIC-WG) transition, electromagnetic bandgap (EBG), multilayer waveguide (MLW), packaged receiver, silicon–germanium (SiGe).**

I. Introduction

SUB-THZ is a key technology in high-data-rate communication systems. With large absolute bandwidth, a sub-THz system can reach up to 100-Gbps data rate in practice, with potential to realize 1 Tbps target in 2030 [1], [2]. Though the performance of sub-THz components has greatly improved over the past years, the delivery of RF signals still needs a practical solution, as traditional contact methods have a worse parasitic effect, leading to increased loss and reduced bandwidth. In addition, integrating transition design based on commercial MMIC's process is also a challenge in sub-THz.

The performance of a transition is related to the specifics of the process and interface. In sub-THz, a printed circuit board (PCB) substrate is available, while still showing high insertion loss and design complexity [3]. Considering a contactless MMIC-WG transition without a direct current path, the key is the realization of an on-chip coupling structure and corresponding matching structures in the waveguide. Antenna-style launchers like bow tie and patch show good transition performance in quartz process [4], [5]. Such structures are easy to utilize in similar processes such as gallium arsenide (GaAs) [6], [7], and indium phosphide (InP) [8], but few of them are integrated with transceivers, especially in sub-THz bands. Silicon-based process, however, can provide a package solution to a fully integrated sub-THz system. Though the conductivity of on-chip metal and resistivity of silicon become extra sources of transition loss [9], proved by previous silicon–germanium (SiGe) BiCMOS solutions [10], [11], techniques like localized backside etching (LBE) can remove silicon under the launcher to reduce the loss [12].

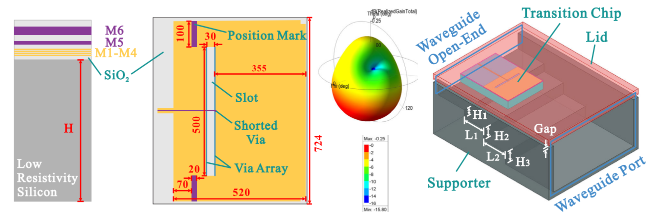

Fig. 1. Core structure and MMIC used in the transition design.

In this letter, a D-band MMIC-WG transition is proposed based on Infineon B11HFC SiGe BiCMOS process with stack-up, as shown in Fig. 1. The core structure of the transition includes a slot in a SiGe chip and steps in a waveguide, realizing contactless coupling and impedance matching, respectively. Electromagnetic bandgap (EBG) structures are introduced to suppress leakage from the possible air gap between different blocks and layers. For fabrication simplicity, the waveguide is sliced into pieces, forming a multilayer waveguide (MLW), with glide-symmetric holes along its transmission channel. As a reference, H-split RWG with pins is used in transition design as well. Measurement results show the proposed transitions achieve low insertion loss and wide bandwidth in the SiGe process. Proved by packaged receiver designs, they can be used for the packaging of SiGe MMIC as well.

II. Analysis and Design

The proposed MMIC to waveguide transition is based on an on-chip slot for electromagnetic coupling and steps in the

Received 17 March 2026; accepted 17 May 2026. This work was supported in part by the Advanced Digitalization Program at the WiTECH Centre HiComIn, financed by VINNOVA, Ericsson, Gapwaves, and Chalmers; and in part by Sweden Vetenskaprådet Project HI-CORE under Grant 2023-05184.
(Corresponding author: Zhongxia Simon He.)

Haojie Chang, Vessen Vassilev, Frida Strömbeck, Yu Yan, and Herbert Zirath are with the Microwave Electronics Laboratory, Chalmers University of Technology, 412 58 Gothenburg, Sweden (e-mail: haojie@chalmers.se).

Zhongxia Simon He is with Chalmers Industriteknik, 412 58 Gothenburg, Sweden, and also with Beijing Institute of Technology, Zhuhai 519087, China (e-mail: simon.he@chalmersindustriteknik.se).
Digital Object Identifier 10.1109/LMWT.2026.3696765

© 2026 The Authors. This work is licensed under a Creative Commons Attribution 4.0 License.
For more information, see https://creativecommons.org/licenses/by/4.0/

This article has been accepted for inclusion in a future issue of this journal. Content is final as presented, with the exception of pagination.

waveguide for impedance matching, as shown in Fig. 1. For chip attachment, the waveguide is split along its H-plane, which makes it difficult to achieve good electrical contact in reality, leading to leakage from the airgap between different blocks. In this letter, pins in an H-split rectangular waveguide (RWG) and glide-symmetric holes in MLW are applied and compared, both showing the ability to suppress the field leakage.

A. Core Transition Design

The core design of the proposed transition can be divided into two parts, namely the chip launcher and waveguide structure.

The on-chip slot is half-wavelength and soldered along the propagation direction of the waveguide for mode matching. It acts as an antenna-style launcher for electromagnetic coupling from the chip to the waveguide. Fig. 1 shows the simulated radiation pattern. A 50 Ω microstrip line on M6 is used for excitation and is shorted by an M6-to-M4 via to avoid the larger size of traditional capacitive-load feeding. The slot in the ground plane occupies M1-to-M4 metal layers, with a surrounding via array to prevent field dissipation between the ground planes.

The quarter-wavelength WG steps are introduced for impedance matching between $Z_S = Z_0 = 50\ \Omega$ on-chip line and the WR-6.5 waveguide with effective characteristic impedance of $Z_L = Z_3 = 247\ \Omega$ [15]. The initial dimensions of the WG steps can be calculated with $Z_1 = 111\ \Omega$ and $Z_2 = 166\ \Omega$ using second order binomial response ($n = 0, 1, \ldots, N$ and $N = 2$) in the following equation:

$$\ln \frac{Z_{n+1}}{Z_n} = 2^{-N} \frac{N!}{(N-n)!n!} \cdot \ln \frac{Z_L}{Z_S}. \quad (1)$$

Calculated from $Z_{diople} \times Z_{slot} = \eta_0^2/4\epsilon_r$ where $\epsilon_r = 4$ is dielectric constant of SiO_2 and $Z_{diople} = 70\ \Omega$ and the impedance of on-chip slot launcher is 127 Ω and a little higher than Z_1 [16]. Simulation software HFSS is applied to optimize the step sizes for a better matching result. Finally, the steps' parameters are $L_1 = 0.4$, $L_2 = 0.45$, $H_1 = 0.14$, $H_2 = 0.2$, and $H_3 = 0.2$ (unit: mm) marked in Fig. 1. Due to different heights of waveguide transmission channels, which will be explained later, the matching results are slightly different in H-split RWG and MLW transition designs, though sharing the same step sizes.

The position of the slot launcher inside the waveguide affects the reverse transmission from the open end of the waveguide; consequently, the return loss. With simulation optimization, the detailed size of the on-chip slot is shown in Fig. 1. In addition, the slot launcher is dielectric loaded with the silicon substrate beneath. Consequently, the thickness of the silicon substrate influences impedance matching, requiring thinning down the silicon wafer or the matching function of stepped waveguide works in other frequencies. As a result, the thickness of the silicon substrate (H) is reduced from the original 185 to 150 μm.

B. Leakage Suppression by EBG

As shown in Fig. 1, the waveguide is split to make possible the assembly. The gap indicated in Fig. 1 introduces leakage

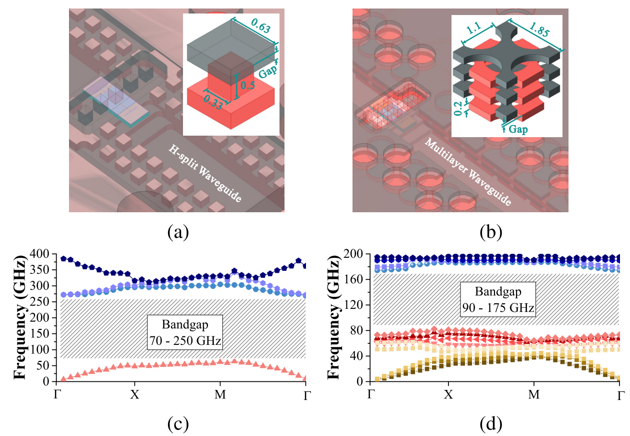

Fig. 2. Pins and glide-symmetric holes used in H-split RWG and MLW with simulated bandgap (gap = 0.01 mm). (a) Pins. (b) Glide-symmetric holes. (c) Pins bandgap. (d) Holes bandgap.

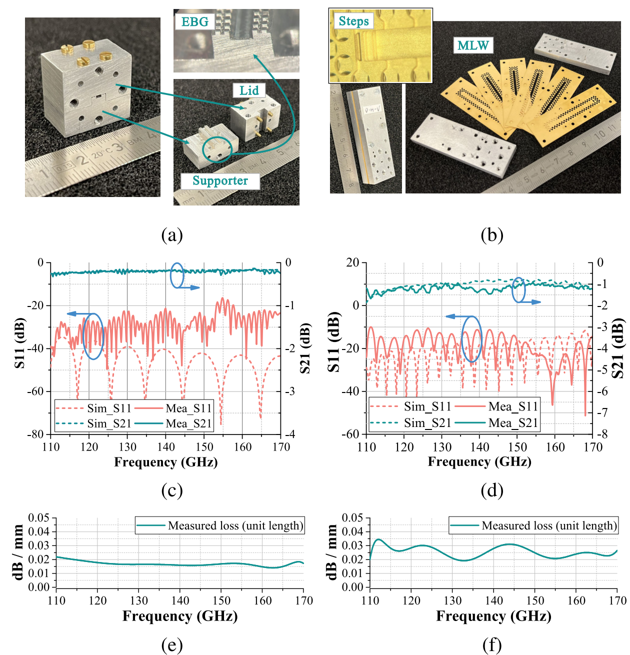

Fig. 3. Experimental results of H-split RWG and MLW with photographs. (a) H-split RWG photographs. (b) MLW photographs. (c) H-split RWG performance. (d) MLW performance. (e) H-split RWG loss. (f) MLW loss.

as it interrupts the current path in the waveguide walls. To mitigate this problem, EBG structures are commonly utilized in suppressing field leakage. Vertical metal pin array, as shown in Fig. 2(a), is one option. With properly parameter setting, pins show a wide stopband in D-band for leakage suppression. The drawback of pins is related to the manufacturing process, restricting their application to higher frequencies.

Instead of machining vertical pins, chemical etching can realize small patterns on a thin metal sheet. The minimum pattern size is related to the thickness of the metal sheet, making it a good candidate for sub-THz waveguide structure fabrication. If the waveguide is realized by sticking several metal layers, leakage from the interface between the layers needs to be addressed. Therefore, glide-symmetric holes are introduced in MLW in practice [13]. As shown in Fig. 2(b), the periodic holes also present a stopband covering the whole D-band, with less difficulty in fabrication.

This article has been accepted for inclusion in a future issue of this journal. Content is final as presented, with the exception of pagination.

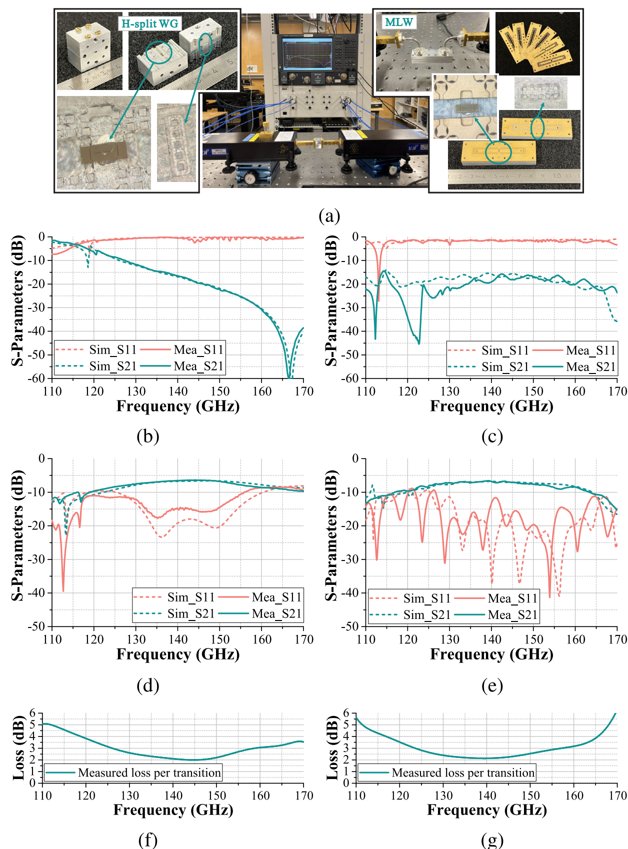

Fig. 4. Simulated and measured results of H-split RWG and MLW B2B transitions with photographs. (a) photographs of B2B transitions with measurement setup. (b) H-split RWG w/o chip. (c) MLW w/o chip. (d) H-split RWG with chip. (e) MLW with a chip. (f) H-split RWG per transition loss. (g) MLW per transition loss.

TABLE I

COMPARISON BETWEEN PROPOSED TRANSITION AND RELEVANT WORKS

Ref.	Process	Freq (GHz)	IL / RL (dB)
[3]	PCB	112 - 170	3 / 10
[4]	Quartz	110 - 170	0.5 / 8.5
[5]	Quartz	118 - 161	2 / 10
[6]	GaAs	85 - 105	0.5 / 10
[7]	GaAs	100 - 135	1 / 5
[10]	SiGe	110 - 139	5 / -
[11]	SiGe	110 - 170	4.2 / 5
This-RWG	**SiGe**	**121 - 155**	**2 / 10**
This-MLW	**SiGe**	**118 - 162**	**2 / 10**

To prove glide-symmetric holes and pins are both feasible in the proposed transition design, a straight H-split RWG with pins and a six-layer MLW with glide-symmetric holes are fabricated and measured, as illustrated in Fig. 3. The H-split RWG has two rows of pins along both transmission sides, with the pins' size given in Fig. 2(a), made of aluminum. To the six-layer MLW, the transmission channel is etched in the middle four copper sheets, covered by the top and bottom sheets. The glide-symmetric holes are introduced in all layers for leakage suppression. Because each copper sheet is 0.2 mm thick according to the etching process, the height of the transmission waveguide in MLW is 0.8 mm if ignoring the airgap, slightly different from the WR-6.5 standard (1.651 $\times$ 0.8255 mm). Its influence on impedance matching is eliminated by optimizing the step sizes, and the connection

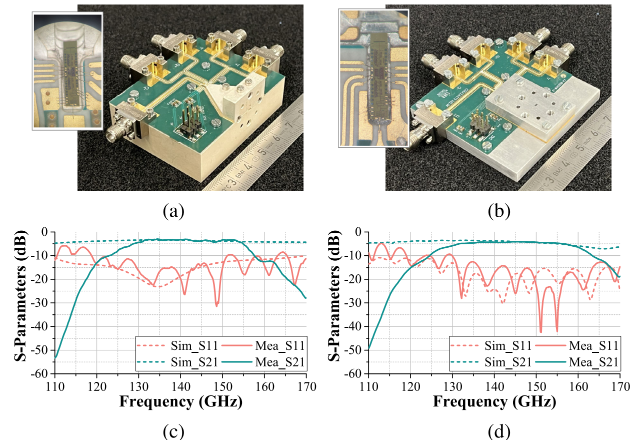

Fig. 5. Measured transition loss in H-split RWG and MLW packaged receivers, compensated by RX gain and IF path loss while including on-chip line loss and waveguide loss. (a) H-split RWG RX. (b) MLW RX. (c) RWG transition loss in RX. (d) MLW transition loss in RX.

with other WG port components is still available by a vertical WR-6.5 interface using a discrete stepped bend structure, as shown in Fig. 3(b). To prevent bending and twisting during measurement, the thin MLW is pressed by two aluminum metal blocks, becoming a sandwiched structure. According to measurement results, the two waveguides both have good transmission performance in D-band, with loss per length (dB/mm) shown in Fig. 3(e) and (f).

III. MEASUREMENT AND INTEGRATION

A. B2B Verification

With the core transition design and leakage suppression techniques presented above, the proposed transition is realized in MLW and also in H-split RWG as a reference. Back-to-back (B2B) structure is chosen for performance verification. To suppress the unwanted waveguide through-mode in the B2B structure, extra pins are added in the lids of the H-split RWG and the top metal block in MLW to reduce coupling between the two waveguide channels. The restricted minimum fabrication size allows only one row of pins in the H-split RWG lid when including the required cavity. However, independent fabrication processes between copper sheets and aluminum blocks in MLW transition make two rows of D-band pins feasible when the cavity is etched in the top sheet. As a result, MLW B2B transition shows better waveguide through-mode suppression, although both of them offer enough suppression within the transition band. The fabricated B2B transitions are shown in Fig. 4(a), together with the measurement setups.

As shown in Fig. 4, the proposed H-split RWG and MLW transitions show 3-dB bandwidth with −10-dB return loss between 120.8–155.8 GHz and 117.9–162.8 GHz, respectively. Compensated by waveguide transmission loss, the two B2B transitions give insertion loss of 6.5 and 6.7 dB at center frequency, proving MLW can be a replacement for H-split RWG with similar performance. Here, the transition loss is increased with several loss contributions, including on-chip transmission line loss, on-chip conductor loss, and dissipation in low-resistivity silicon substrate. The on-chip line loss of 2.58 dB is partly due to the conductivity of the chip metal layers. Thus, the per transition loss is calculated to be 1.96 and 2.06 dB in H-split RWG and MLW design, respectively. The

This article has been accepted for inclusion in a future issue of this journal. Content is final as presented, with the exception of pagination.

on-chip metal conductivity and silicon resistivity are process-based, leading to bandwidth reduction and loss increment, and consequently account for over 70% transition loss compared with simulation using ideal on-chip conditions. Table I gives the comparison between the proposed transitions and relevant work found in the literature.

B. Packaged Receivers

The H-split RWG and MLW transitions are then applied in the package of a D-band receiver [14], as shown in Fig. 5. The radio frequency (RF) signal is received by the on-chip slot, directly cascaded at the input of the low-noise amplifier in RX. The local oscillator (LO) and intermediate frequency (IF) pads are connected to transmission lines on a 10-mil-thick RO4350B PCB by wire bonding. The sizes of H-split RWG and MLW packaged receivers are $56.8 \times 46 \times 25.8$ and $56.6 \times 55.6 \times 12.2$ (unit: mm), respectively. Measured results are presented in Fig. 5, compensated by on-chip measured RX conversion gain and IF path loss. They represent the practical transition loss, including extra on-chip line and waveguide loss, when using the proposed H-split RWG and MLW transition in a real D-band system.

Referring to Figs. 4 and 5, MLW-based transition shows the same insertion loss as H-split RWG design. Though the assembly needs extra stages, the MLW solution shows easier EBG fabrication, leading to lower cost and higher stability. In addition, the MLW package solution is more flexible in integrating with active circuits or antennas due to its sliced metal pieces, helping to avoid being divided into more blocks.

IV. Conclusion

In this letter, a MMIC-WG transition is proposed based on the SiGe process and MLW technology. A slot in the ground plane integrated onto the MMIC and impedance matching steps in the waveguide constitute the transition structure. Pins and glide-symmetric holes are introduced to reduce leakage from split metal blocks and layers. Compared with the H-split RWG transition, the proposed MLW transition shows the same performance, but is more flexible in assembly and cost efficient. The proposed transition is used to package an RX MMIC, showing applicability in future sub-THz communication systems.

Acknowledgment

The authors would like to thank Infineon Technologies for the fabrication of the chips.

References

[1] Y. Kim et al., “150-GHz CMOS TX/RX with digitally predistorted PAM-4 modulation for terahertz contactless/plastic waveguide communications,” *IEEE Trans. THz Sci. Technol.*, vol. 10, no. 4, pp. 370–382, Jul. 2020.

[2] K. Dens et al., “Design of a noncoherent 100-Gb/s 3-m dual-band PAM-4 dielectric waveguide link in 28-nm CMOS,” *IEEE J. Solid-State Circuits*, vol. 59, no. 5, pp. 1398–1408, May 2024.

[3] C. Liu et al., “A 640-Gb/s 4× 4-MIMO D-band CMOS transceiver chipset,” *IEEE J. Solid-State Circuits*, vol. 60, no. 4, pp. 1132–1149, Apr. 2025.

[4] Z. Liu, Y. Yao, Z. Liu, Q. Li, and X. Cheng, “Sub-THz inline transition from microstrip line to waveguide for large-sized MMICs,” *IEEE Trans. Compon., Packag., Manuf. Technol.*, vol. 14, no. 8, pp. 1474–1480, Aug. 2024.

[5] Y. Dong, T. K. Johansen, V. Zhurbenko, and P. J. Hanberg, “A rectangular waveguide-to-coplanar waveguide transition at D-band using wideband patch antenna,” in *Proc. 48th Eur. Microw. Conf. (EuMC)*, Madrid, Spain, Sep. 2018, pp. 1045–1048.

[6] A. R. Vilenskiy and Y. Zhang, “A compact and wideband MMIC-to-ridge gap waveguide contactless transition for phased array antenna front ends,” *IEEE Antennas Wireless Propag. Lett.*, vol. 23, pp. 990–994, 2024.

[7] A. Hassona, Z. S. He, V. Vassilev, and H. Zirath, “F-band low-loss tapered slot transition for millimeter-wave system packaging,” in *Proc. 49th Eur. Microw. Conf. (EuMC)*, Paris, France, Oct. 2019, pp. 432–435.

[8] H. Zhu, Y. Zhang, C. Wu, F. Xiao, R. Xu, and B. Yan, “Integrated dipole antenna with bandwidth enhancement for terahertz waveguide-to-CPWG transition,” *IEEE Antennas Wireless Propag. Lett.*, vol. 19, pp. 2433–2436, 2020.

[9] P. Kaul, A. Aljarosha, A. B. B. Smolders, P. Baltus, M. Matters-Kammerer, and R. Maaskant, “An E-band silicon-IC-to-waveguide contactless transition incorporating a low-loss spatial power combiner,” in *Proc. Asia Pacific Microw. Conf. (APMC)*, Kyoto, Japan, Nov. 2018, pp. 1528–1530.

[10] Z. Simon He et al., “A 140 GHz transmitter with an integrated chip-to-waveguide transition using 130 nm SiGe BiCMOS process,” in *Proc. Asia Pacific Microw. Conf. (APMC)*, Kyoto, Japan, Nov. 2018, pp. 28–30.

[11] J. Campion et al., “Toward industrial exploitation of THz frequencies: Integration of SiGe MMICs in silicon-micromachined waveguide systems,” *IEEE Trans. THz Sci. Technol.*, vol. 9, no. 6, pp. 624–636, Nov. 2019.

[12] F. Xie, Z.-C. Hao, Z. Li, and Z. Chen, “A 220-GHz perpendicular chip-to-waveguide transition using an LBE-SiGe-based cavity,” *IEEE Microw. Wireless Technol. Lett.*, vol. 33, no. 9, pp. 1266–1269, Sep. 2023.

[13] A. Vosoogh, H. Zirath, and Z. S. He, “Novel air-filled waveguide transmission line based on multilayer thin metal plates,” *IEEE Trans. Terahertz Sci. Technol.*, vol. 9, no. 3, pp. 282–290, May 2019.

[14] F. Strömbeck, Y. Yan, and H. Zirath, “A beyond 100-gbps polymer microwave fiber communication link at D-band,” *IEEE Trans. Circuits Syst. I, Reg. Papers*, vol. 70, no. 7, pp. 3017–3028, Jul. 2023.

[15] F. Ishihara and S. Iiguchi, “Equivalent characteristic impedance formula of waveguide and its applications,” *Electron. Commun. Jpn., II, Electron.*, vol. 75, no. 5, pp. 54–66, Jan. 1992.

[16] W. Stutzman and G. Thiele, *Antenna Theory and Design*. Hoboken, NJ, USA: Wiley, 2012, pp. 244–245.